IEEE Access
Multidisciplinary | Rapid Review | Open Access Journal

Received December 10, 2021, accepted January 16, 2022, date of publication January 21, 2022, date of current version February 1, 2022.

Digital Object Identifier 10.1109/ACCESS.2022.3145583

Recurrent NEAT Assisted 2D-DOA Estimation With Reduced Complexity for Satellite Communication Systems

YUNFENG LI[1,2], (Student Member, IEEE), YONGHUI HUANG[2], GERT FRØLUND PEDERSEN[3], (Senior Member, IEEE), AND MING SHEN[3], (Senior Member, IEEE)

[1]National Space Science Center, Chinese Academy of Sciences, Beijing 100190, China
[2]School of Electronic, Electrical and Communication Engineering, University of Chinese Academy of Sciences, Beijing 100049, China
[3]Department of Electronic Systems, Aalborg University, 9220 Aalborg, Denmark

Corresponding author: Yonghui Huang (yonghui@nssc.ac.cn)

This work was supported by the China Scholarship Council under Grant 202004910734.

ABSTRACT Direction-of-arrival (DOA) estimation plays a vital role in the field of array signal processing. However, the need for heavy computing tasks in most traditional DOA algorithms, e.g., multiple signal classification (MUSIC), makes their engineering practicality significantly compromised in satellite communication systems. The neuroevolution of augmenting topologies (NEAT) can quickly search for appropriate topologies and weights of neural network functions, but its computational complexity is still too high for satellite systems. This paper proposes a modified NEAT architecture featuring a recurrent structure (RNEAT) that only needs a small number of phase components of the received signal covariance matrix as inputs to reduce the complexity and simplify the neural network architecture. The proposed RNEAT incorporated with multiple signal classification (RNEAT-MUSIC) features low complexity to achieve high resolution and low complexity simultaneously. Validation has been done by applying the proposed method in a two-dimensional direction of arrival estimation (2D-DOA) problem. Results show that the proposed RNEAT-MUSIC efficiently restricts the scanning region before forwarding the covariance matrix to the MUSIC stage. Consequently, the computational workload is reduced by 3/4 compared with the traditional 2D-MUSIC algorithm while maintaining satisfactory DOA resolution.

INDEX TERMS Direction-of-arrival (DOA), neuroevolution of augmenting topologies (NEAT), multiple signal classification (MUSIC), RNEAT-MUSIC, satellite communication.

I. INTRODUCTION

Orbiting satellites and other space vehicles have complex trajectories, and ground stations need to acquire their angular positions quickly and accurately. Under normal circumstances, this can be solved by a complex trajectory estimation model. However, antenna arrays in ground sections need to have high gain, which results in a narrow beam and a prolonged period to acquire the accurate data of satellites [1]. Especially under certain scenarios (e.g., launch and early orbit phase (LEOP) of critical maneuvers), ground stations will lose the ability to operate the spacecraft [2]. Besides, radio frequency interference (RFI) incidents from the ground to satellites show an upward trend [3], [4]. Therefore, for array signal processing in LEOP and low earth orbit (LEO) satellites, reliable and fast direction of arrival (DOA) estimation techniques should be considered.

The DOA estimation analyzes target sources' position based on incident signals received by the antenna array [5]. The two-dimensional direction of arrival (2D-DOA) estimation based on the uniform rectangular array (URA) is more suitable for practical application environments than the one-dimensional uniform linear array (ULA) [6]. Therefore, over the past few decades, many high-resolution 2D-DOA estimation algorithms have been proposed [7]–[18]. The most representative ones are the multiple signal

The associate editor coordinating the review of this manuscript and approving it for publication was Chao Tong.

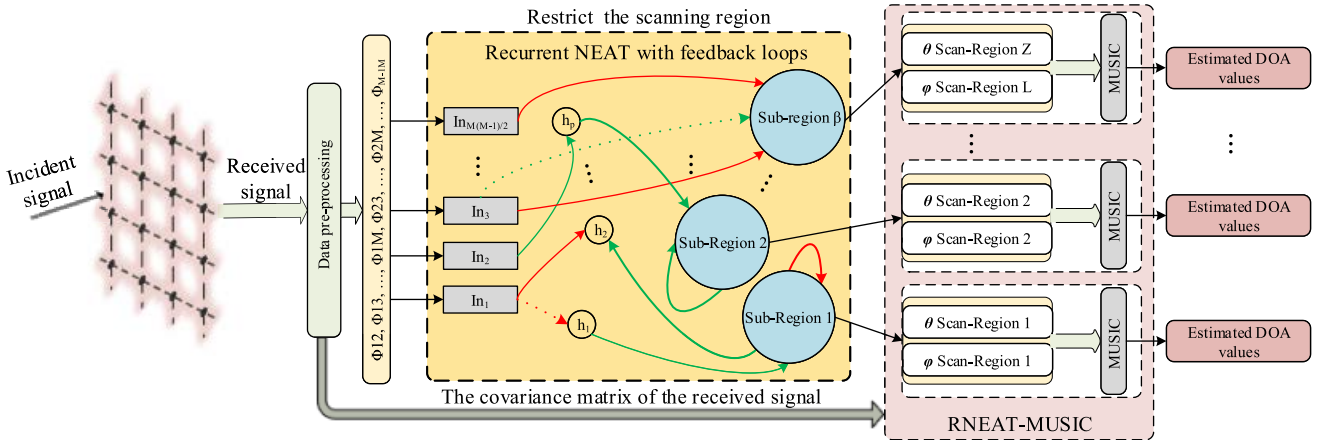

FIGURE 1. The recurrent NEAT incorporates with multiple signal classification (RNEAT-MUSIC) for 2D-DOA.

classification (MUSIC) algorithm [7] and the estimation of signal parameters via rotational invariance techniques (ESPRIT) [8]. The ESPRIT algorithm does not need peak search, while it has restrictions on the array structure [20]. The MUSIC algorithm obtains mutually orthogonal signal subspace and noise subspace by performing eigenvalue decomposition (EVD) on the array output covariance matrix. It then estimates the signal DOA through peak search. Since the signal subspace and the noise subspace are completely orthogonal under the noise-free model, MUSIC theoretically features super-resolution for arbitrarily close targets. It can be applied in a different type of antenna array [19]. Therefore, MUSIC has wider engineering practicality. However, the excessive calculation amount for two-dimensional peak search is one of the main factors hindering the progress of its application.

Machine learning has been proven to effectively optimize the computational complexity of the 2D-MUSIC algorithm, which can be divided into two cases [21]. In one situation, the number of signal sources should be acquired in advance. In [22], the authors propose a deep neural network (DNN) based massive multi-input multi-output (MIMO) framework. Furthermore, The DNN achieves end-to-end learning for super-resolution DOA estimation based on nonlinear mapping operations. Nevertheless, what hinders its generalization is the requirement of source numbers as prior knowledge [22]. Simultaneously, this is also the general deficiency of several related works [23]–[26].

Nevertheless, the source number is unknown in a general application scenario. So, in another situation, the first step of DOA estimation becomes a multi-label classification task. Neural networks are relatively convenient as a classification modeling tool since they can learn from the present data [27]. One of the significant trends for recent works is to use the backpropagation neural network, e.g., gradient descent [28]. This case has been studied in [29], where a two-stage DNN structure is proposed. The proposed framework consists of a multitask autoencoder and a series of parallel multilayer classifiers, which realizes the super-resolution DOA estimation and channel estimation. However, only the two-signal-source case is considered in the training process, resulting in unsatisfactory performances under different signal numbers. Apart from the aforementioned lacking, most previous machine learning-based studies estimate sources with signal angular distance $\triangle\theta = 5^\circ$ [30] or even $\triangle\theta = 10^\circ$ [31]. Besides, designing neural networks architecture and its optimization is challenging.

This work targets on minimizing the neural network and setting the weights automatically, so the evolutionary algorithm is employed to discover such networks. This neural network is close to the biological neural network system [32]. Being similar to biological neural networks, it does not need the step of backpropagation. The way to dominate it to solve problems is evolution. The implementation of neuroevolution presented in this paper relies on neuroevolution of augmenting topologies (NEAT) to automate the search for appropriate topologies and weights of neural network function [33]. NEAT is an appropriate choice because of its ability to optimize network topologies automatically.

This paper proposes a recurrent NEAT incorporate with MUSIC (RNEAT-MUSIC) to reduce the computational complexity of the 2D-DOA of signal sources, as shown in Fig. 1. The primary contributions of this paper are outlined as follows:

- A modified NEAT architecture featuring a recurrent structure (RNEAT) is proposed that only needs a small number of phase components of the received signal covariance matrix as inputs to reduce the complexity and simplify the neural network architecture.
- The proposed RNEAT-MUSIC efficiently restricts the scanning region before forwarding the covariance matrix to the MUSIC stage.
- The proposed RNEAT-MUSIC can be easy to achieve high resolution and low complexity simultaneously.
- The computational workload is reduced by 3/4 compared with the traditional 2D-MUSIC algorithm while maintaining superior DOA resolution/performance.

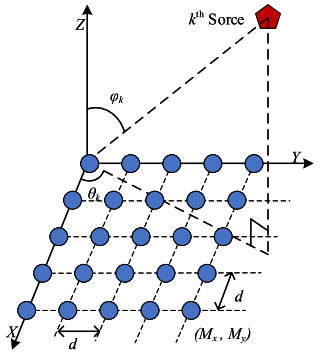

FIGURE 2. The structure model of uniform rectangular array.

This paper is organized as follows. The received signal model and conventional 2D-MUSIC are presented in Section II. A detailed description of the proposed framework is presented in Section III. The simulation results of the RNEAT-MUSIC algorithm for DOA estimation are presented in Section IV. Section V concludes this work.

II. MATHEMATICAL FORMULATION

A. SIGNAL MODEL

In Fig. 2, it is assumed that K narrow-band non-coherent signals impinge on a uniform rectangular array (URA). The numbers of array elements in X and Y directions are M_x and M_y, respectively. Variables θ_k and φ_k represent the azimuth angle and elevation angle of the k^{th} incident signal source to the antenna array, where $\theta_k \in [0, 2\pi]$ and $\varphi_k \in \left[0, \frac{\pi}{2}\right]$. The received data of the antenna array at time instant t can be expressed as

$$X(t) = \sum_{k=1}^{K} a(\theta_k, \varphi_k) s_k(t) + N(t), \tag{1}$$

where $s_k(t)$ is the signal source transmitted by the k^{th} source, and $N(t)$ is the additive white Gaussian noise (AWGN) vector. It is assumed that the noise and signals are uncorrelated. The steering vector of the k^{th} source is represented by $a(\theta_k, \varphi_k)$.

It is supposed that

$$\begin{cases} u_k = 2\pi d \cos\theta_k \sin\varphi_k / \lambda \\ v_k = 2\pi d \sin\theta_k \sin\varphi_k / \lambda, \end{cases} \tag{2}$$

where d $(= \frac{\lambda}{2})$ is inter-element spacing, and λ is the wavelength of the signal incidents on the antenna array. The m^{th} antenna element of the steering vector is defined as

$$[a(\theta_k, \varphi_k)]_m = exp\left(j[u_k(m_x - 1) + v_k(m_y - 1)]\right), \tag{3}$$

where $m_x = 1, 2, \ldots, M_x$ and $m_y = 1, 2, \ldots, M_y$ are the row number and column number of the m^{th} antenna element, respectively.

The matrix form of $X(t)$ can be rewritten as

$$X(t) = AS(t) + N(t), \tag{4}$$

where $A = [a(\theta_1, \varphi_1), \ldots, a(\theta_K, \varphi_K)]$ and $S(t) = [s_1(t), s_2(t), \ldots, s_K(t)]^T$ are the steering matrix and signal vector, respectively.

B. CONVENTIONAL 2D-MUSIC

The covariance matrix of the antenna array received data is defined as

$$\begin{aligned} R &= E\left[X(t)X(t)^H\right] = AE\left[S(t)S(t)^H\right]A^H + \sigma^2 I \\ &= AR_S A^H + \sigma^2 I, \end{aligned} \tag{5}$$

where $E[\cdot]$ represents the statistical expectation. Due to that the signal and noise are independent of each other, the covariance matrix can be decomposed into signal and noise parts. The term $AR_S A^H$ denotes the signal part, where R_S is the covariance matrix of the signal, and H represents the complex conjugate transpose. Variables σ^2 and I indicate the AWGN power and unit matrix, respectively.

After the eigen decomposition, R can be written as

$$R = U_S \Sigma_S U_S^H + U_N \Sigma_N U_N^H, \tag{6}$$

where U_S and U_N represent the subspace of signal and noise, respectively. Ideally U_S and U_N are mutually orthogonal, so the steering vector of the signal subspace has the following relationship with the noise subspace:

$$a^H(\theta, \varphi) U_N = 0. \tag{7}$$

Actually, the data covariance matrix is replaced by the sampling covariance matrix $\hat{R}$, and

$$\hat{R} = \frac{1}{C} \sum_{c=1}^{C} XX^H, \tag{8}$$

where C indicates the snapshots. By the eigen decomposition of $\hat{R}$, the signal subspace eigenvector matrix $\hat{U}_S$, noise subspace eigenvector matrix $\hat{U}_N$, and diagonal matrix $\hat{\Sigma}$ composed of eigenvalues are obtained as

$$\hat{R} = \hat{U}_S \hat{\Sigma}_S \hat{U}_S^H + \hat{U}_N \hat{\Sigma}_N \hat{U}_N^H. \tag{9}$$

However, $a(\theta, \varphi)$ and $\hat{U}_N$ are not completely orthogonal, due to the presence of noise. Therefore, the DOA is implemented with a minimum optimization search range

$$(\theta, \varphi)_{MUSIC} = arg_{(\theta,\varphi)} min\left[a^H(\theta, \varphi) \hat{U}_N \hat{U}_N^H a(\theta, \varphi)\right], \tag{10}$$

where $\theta \in [0, 2\pi]$ and $\varphi \in \left[0, \frac{\pi}{2}\right]$. Hence the spectrum estimation of the 2D-MUSIC algorithm is obtained as

$$P_{2D-MUSIC}(\theta, \varphi) = \frac{1}{a^H(\theta, \varphi) \hat{U}_N \hat{U}_N^H a(\theta, \varphi)}. \tag{11}$$

The spatial spectrum function $P_{2D-MUSIC}(\theta, \varphi)$ shows a peak at the estimated DOA.

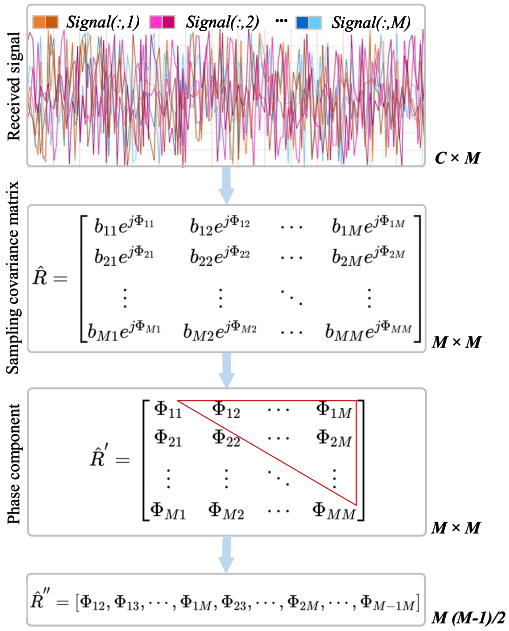

FIGURE 3. The pre-processing of the received signal.

III. THE PROPOSED FRAMEWORK

This paper proposes RNEAT-MUSIC to reduce the computational complexity of 2D-DOA of signal sources, as shown in Fig. 1. First, the phase component of the received signal covariance matrix is extracted, and the reduced dimensional RNEAT-MUSIC is utilized to estimate the 2D-DOA. The improved NEAT algorithm combined with the recurrent structure is used to minimize the neural network and set the weights automatically. The task of restricting scanning regions can be transferred to a supervised multi-class classification work. The possible DOAs are divided into discrete sets, which are noted as sub-regions. The process of RNEAT-MUSIC is described in detail in the following subsections.

A. THE PRE-PROCESSING OF THE RECEIVED SIGNAL

The division of sub-regions is decided from the received signal $X(t)$, as it is indicated in (4). The total number of array elements is $M = M_x \times M_y$. The pre-processing of the received signal is shown in Fig. 3. Each signal, i.e., $Signal(:, 1), Signal(:, 2), \ldots, Signal(:, M)$, represents the received signal at the corresponding antenna element. The sampling covariance matrix $\hat{R}$ is an $M \times M$ complex matrix, and each element of $\hat{R}$ can be represented by amplitude and phase components. The amplitude components are not mandatory for training because much useful information for DOA estimation is included in the phase differences between antenna array elements [35], [36]. Therefore, an $M \times M$ phase component $\hat{R}'$ is extracted. Since the sampling covariance matrix $\hat{R}$ is a symmetric matrix, the upper triangle part of $\hat{R}'$ is sufficient to capture the information of the existing sub-region. The upper triangle part of $\hat{R}'$ can be organized to a vector $\hat{R}''$ with the size of $M(M-1)/2$. The restricted scanning region network is fed with the reshaped form of $\hat{R}''$, which is the input of the NEAT algorithm.

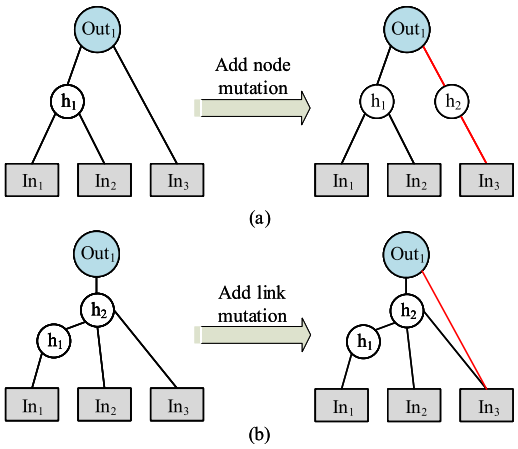

FIGURE 4. The two types of structural mutation in NEAT [40]. (a) Mutation by adding nodes. (b) Mutation by adding lines.

TABLE 1. Key steps of the NEAT algorithm.

Algorithm: The improved 2D-DOA estimation algorithm
*Step*1: Use innovation number to code the neural network;
*Step*2: Crossover based on innovation number;
*Step*3: Make genes mutation to neurons (nodes) and neural links;
*Step*4: Minimize the size of the neural network by initializing the neural network with the simplest architecture where the input can directly connect to the output.

B. NEAT ALGORITHM WITH RECURRENT LINK

The implementation of neuroevolution presented in this paper relies on the NEAT algorithm with recurrent links to automate the search for appropriate topologies and weights of neural network function. The NEAT starts the evolution with a uniform population of minimal structures, i.e., fully connected networks with few hidden nodes. It evolves more complex networks by introducing new nodes and connections through structural mutations, as shown in Fig. 4 [40]. For example, a new node h_2 is added to Fig. 4(a), which is a mutation node on the original link, then the original $In_3 \rightarrow Out_1$ link will be disabled. If the added link is a mutation link, the $In_3 \rightarrow Out_1$ link will be enabled, as shown in Fig. 4(b). A comprehensive explanation of mutation can be found in [33], [41].

The key steps of the NEAT algorithm are shown in Table 1. An example of mutation for the NEAT algorithm with Parent 1 and Parent 2 is shown in Fig. 5. Parent 1 and Parent 2 are the minimal structures of initial evolution. Each link has an exclusive innovation number. First, the innovation number is used to code the neural network directly. The link indicates the status between two nodes, which can be either enabled or disabled. Then networks Parent 1 and Parent 2 crossover based on innovation number, which makes the gene mutation. The innovation number aligns with the two parents. If both parents exhibit the identical innovation number, one

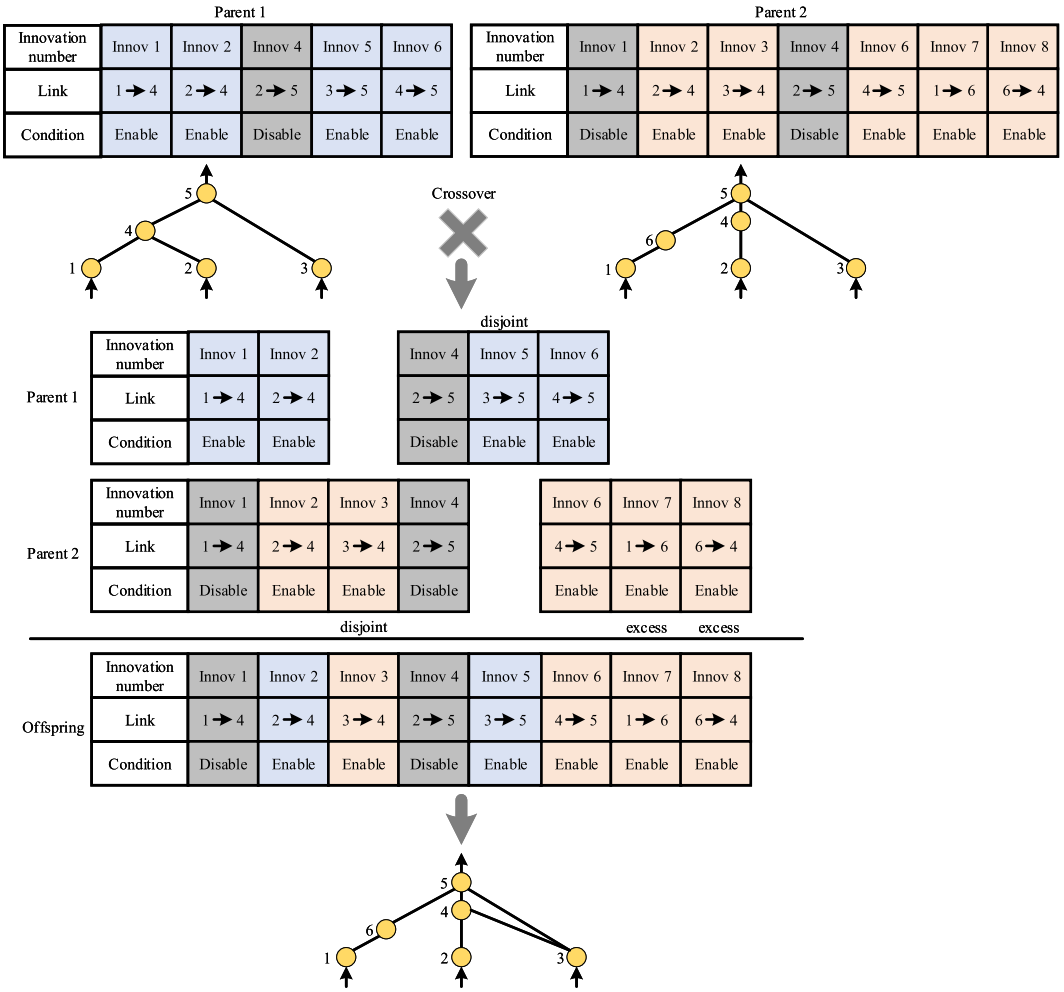

FIGURE 5. An example of mutation for NEAT algorithm.

will be randomly selected. If either one exhibits the innovation number, it will be directly transmitted to the offspring. The offspring is the updated network after the mutation of Parent 1 and Parent 2. The neural network structures are differentiated by "disjoint" and "excess", which are used to distinguish the different degrees of the network. When selecting the neural network structures to be retained, it needs to be calculated by "disjoint" and "excess". The specific calculation method can be found in [42]. Finally, the size of the neural network is minimized by initializing the neural network with the simplest architecture where the input can directly connect to the output.

As shown in Fig. 6, the implementation of neuroevolution presented in this paper relies on the NEAT algorithm with recurrent link to automate the search for appropriate topology and weights of the neural network function [43]. In Fig. 6, the dashed lines represent disabled links, while the solid lines exhibit enabled links. Moreover, the red lines represent links with weight < 0, and the green lines represent links with weight > 0. The thickness of the line exhibits the size

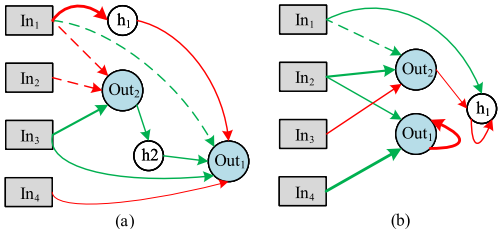

FIGURE 6. The NEAT algorithm (the thickness of the line exhibits the size of the weight). (a) Without recurrent links. (b) With recurrent links.

of the weight in Fig. 6. Compared with Fig. 6(a), Fig. 6(b) has recurrent nodes, such as h_1 and Out_1. The setup with recurrent nodes makes the neural network more diverse and the structure more simplified, and the neural network will produce memory functions. In the prior art, the conventional recurrent neural network (RNN) transmits the memory by hidden layers. Being different from RNN, the recurrent in the NEAT algorithm is a delayed refresh form [33].

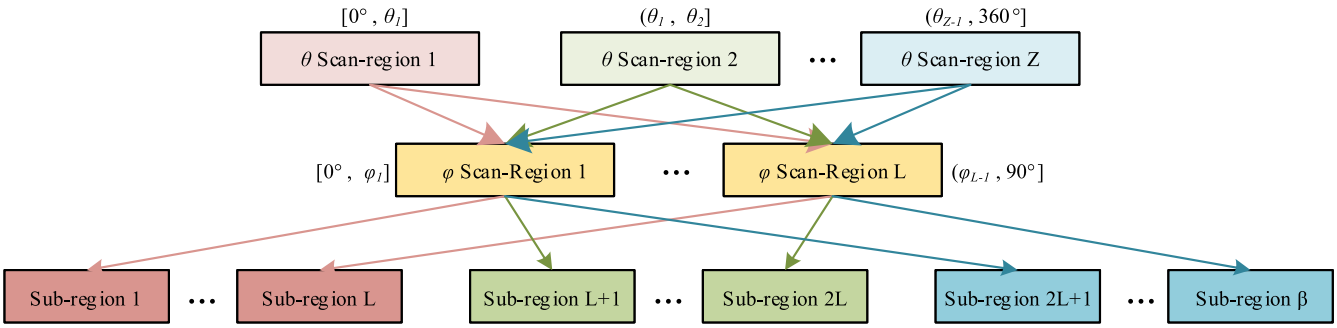

FIGURE 7. Arrangement order of sub-regions.

TABLE 2. Summary of the RNEAT-MUSIC algorithom.

Algorithm: The proposed RNEAT-MUSIC estimation algorithm
*Step*1: The data covariance matrix R is obtained from the received data of antenna array;
*Step*2: The data covariance matrix is replaced by the sampling covariance matrix $\hat{R}$;
*Step*3: The reshaped form of $\hat{R}''$, as shown in Fig. 3, is fed into the improved neuroevolution NEAT algorithm;
*Step*4: The improved neuroevolution NEAT algorithm combined with recurrent structure is used to minimize the restricted scanning region's neural network and automatically set the weights;
*Step*5: The sub-region is obtained, and transmit the information to the MUSIC algorithm;
*Step*6: Identify the angle in the sub-region corresponding to the maximum points, which are the signal sources incident directions.

C. THE PROPOSED RNEAT-MUSIC AND COMPUTATIONAL COMPLEXITY ANALYSIS

The summary of the proposed RNEAT-MUSIC algorithm is presented in Table 2. To illustrate the computational complexity of the proposed algorithm, comparisons of the classic 2D-MUSIC [7], unitary MUSIC (U-MUSIC) [34], and real-valued MUSIC (RV-MUSIC) [35] are shown in Table 3. As mentioned above, M and K indicate the total numbers of array elements and signal sources, respectively. Variables J_Θ and J_Ψ denote the sample search points along with θ and φ directions, respectively. The complexity unit is usually represented by $\mathcal{O}[\cdot]$. The common term $\mathcal{O}[M^2K]$ presents the complexity of the eigenvalue decomposition (EVD) step on an $M \times M$ matrix by using the fast subspace decomposition (FSD) technique [39]. Because the 2D-MUSIC after EVD calculation is a complex matrix, the common term $\mathcal{O}[M^2K]$ for 2D-MUSIC is given by $4 \times \mathcal{O}[M^2K]$. Since $a(\theta, \varphi) \in \mathbb{C}^{M\times 1}$ and $\hat{U}_N \in \mathbb{C}^{M\times(M-K)}$ in (10), computing the 2D-MUSIC spectrum for $(J_\Theta J_\Psi)$ sample points over full scan region costs $4 \times \mathcal{O}[J_\Theta J_\Psi (M+1)(M-K)]$ flops [7]. The U-MUSIC needs to take into account that $a_{real}(\theta, \varphi) \in \mathbb{R}^{M\times 1}$, $a_{imag}(\theta, \varphi) \in \mathbb{R}^{M\times 1}$, and $\hat{U}_N \in \mathbb{R}^{M\times(M-K)}$ [34]. The RV-MUSIC reduces the search range by half, so the complexity of spectrum for RV-MUSIC is reduced to $\mathcal{O}\left[J_\Theta J_\Psi (M+1)(M-2K) + 5 \times M^2K\right]$ [35].

The proposed method involves a compressed search over a sub-region, and it only computes $(J_\Theta J_\Psi)/\beta$ samples, where β is the number of restricted scan regions. The arrangement sequence of sub-regions is shown in Fig. 7. The θ scan-region 1 combined with each φ scan-region (φ scan-region 1 to L) to form sub-region 1 to L, and so on. It can be observed from Table 3 that the U-MUSIC and RV-MUSIC have comparable computational complexities, and both of them have much lower complexities than the conventional 2D-MUSIC. In massive antenna array systems, the relationship $J_\Theta J_\Psi \gg M > K$ usually exists. Therefore, the algorithm complexity ratio of RNEAT-MUSIC and 2D-MUSIC can be approximated as

$$\mathcal{R} \approx \frac{4 \times \mathcal{O}\left[J_\Theta J_\Psi/\beta\,(M+1)(M-K)\right]}{4 \times \mathcal{O}\left[J_\Theta J_\Psi\,(M+1)(M-K)\right]} \approx \frac{1}{\beta}. \quad (12)$$

When $\beta = 4$, $\mathcal{R} \approx 1/4$ can be obtained. It means that the computational complexities are reduced by 3/4 under the case $\beta = 4$, where similar performances can also be found in [34], [35]. Under the case $\beta > 4$, more than 3/4 of computational complexities can be reduced by the proposed RNEAT-MUSIC compared with the classical 2D-MUSIC.

A comparison of the network structural complexity among several DOA estimation algorithms is presented in Table 4. DNN [22] and CNN [36] both have three hidden layers and

TABLE 3. Comparisons of RNEAT-MUSIC computational complexity (Comparison with the classical 2D-MUSIC, where the complexity of the proposed RNEAT-MUSIC technique is more than 3/4 lower under the case $\beta > 4$).

Scheme	Computational complexity
2D-MUSIC [7]	$4 \times \mathcal{O}\left[J_\Theta J_\Psi (M+1)(M-K) + M^2K\right]$
U-MUSIC [34]	$\mathcal{O}\left[J_\Theta J_\Psi (M+1)(M-K) + M^2K\right]$
RV-MUSIC [35]	$\mathcal{O}\left[J_\Theta J_\Psi (M+1)(M-2K) + 5 \times M^2K\right]$
Proposed	$4 \times \mathcal{O}\left[J_\Theta J_\Psi/\beta\,(M+1)(M-K) + M^2K\right]$

TABLE 4. Comparison of network structural complexity among different DOA estimation algorithms ('W/O' means 'Without' and 'W' means 'With').

Scheme	Quantity of hidden neurons
DNN [22]	45-22-270
CNN [36]	128-128-128
CNN [37]	256-256-256-256
NEAT W/O Recurrent link	273 (no layer)
NEAT W Recurrent link	148 (no layer)

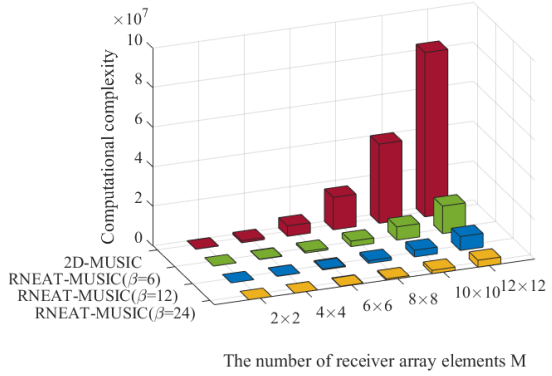

FIGURE 8. Computational complexity of different algorithms versus the number of receiver array elements (i.e., 2 × 2, 4 × 4, 6 × 6, 8 × 8, 10 × 10, and 12 × 12) with 100 trials under SNR = 10 dB.

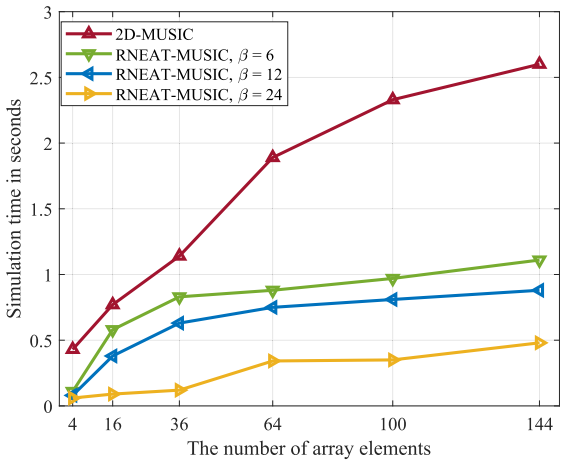

FIGURE 9. Simulation time versus the number of array elements (i.e., 2 × 2, 4 × 4, 6 × 6, 8 × 8, 10 × 10, and 12 × 12) with 100 trials under SNR = 10 dB.

more than 330 hidden neurons. The CNN [37] has four hidden layers and 1024 hidden neurons. The NEAT without recurrent link has 273 hidden neurons. It can be observed that NEAT has a much simpler structure than DNN and CNN, since there is no concept of layer, only hidden nodes. Moreover, the structure of recurrent link is added in this work to further reduce the hidden nodes as well as to simplify the network structure. Specifically, the NEAT with recurrent link only has 148 hidden neurons in the network structure. Additionally, it can automatically set the weight and network structure, which saves time for the network optimization.

Fig. 8 shows the computational complexity of the 2D-MUSIC and RNEAT-MUSIC with different β values. It can be seen that the computational complexity of 2D-MUSIC and RNEAT-MUSIC both increase with the increase of array elements number, and the RNEAT-MUSIC requires a much lower computational burden than 2D-MUSIC, especially when the number of receiver array elements is large. The computational complexity of the proposed RNEAT-MUSIC varies with the value of β. Fig. 9 indicates the consumed time of the different β values in

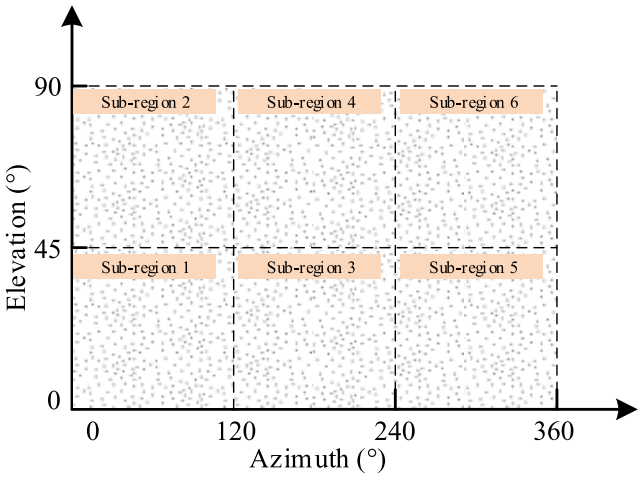

FIGURE 10. 2-D sub-region coordinate system with $\beta = 6$.

TABLE 5. RNEAT-MUSIC for 2D-DOA estimation simulation setup (If not specifically stated, other parameters are as follows).

Parameter	Description
Signal source	Independent narrow-band signals
2D-DOA	$(30°, 15°)$, $(30°, 25°)$
SNR	5 dB
Noise	AWGN
Snapshots	200
Number of receiver array element	5×5
The element spacing	$\lambda/2$
β	6

correspondence with the number of array elements. The calculation is performed in a computer with Intel Core i9 @2.3 GHz CPU and 32 GB RAM by running the MATLAB (Ver. R2020a) codes in the same environment. Signal DOAs $(10°, 20°)$ and $(30°, 40°)$ are incident on a URA. The scan sub-region is $[0°, +120°]$ in azimuth and $[0°, +45°]$ in elevation, and the search step is 0.1. One hundred Monte Carlo trials are carried out with 1000 snapshots and 10 dB signal-to-noise ratio (SNR). It indicates that the RNEAT-MUSIC algorithm has a much lower computational complexity than the 2D-MUSIC algorithm, especially when large number of array elements exist. With the increase of β, the computational complexity is also reduced. If $\beta \to \infty$, and the resolution of the sub-region continues to improve, the DOAs of the signal source can be directly evaluated. This means that it takes a lot of training network process to replace the traditional DOA algorithm. Hence, the division of sub-scanning regions needs to be balanced with the actual application scenarios.

IV. SIMULATION RESULTS AND ANALYSIS

A. RNEAT-MUSIC ALGORITHM FOR 2D-DOA ESTIMATION

The first simulation shows how the RNEAT-MUSIC algorithm recognizes two signals under the 5 dB SNR case, as shown in Table 5. Two independent narrow-band signals with AWGN are studied. Their incident azimuth angle is 30°, and the incident elevation angles are 15° and 25°, respectively. The 2-D sub-region coordinate system with $\beta = 6$ is

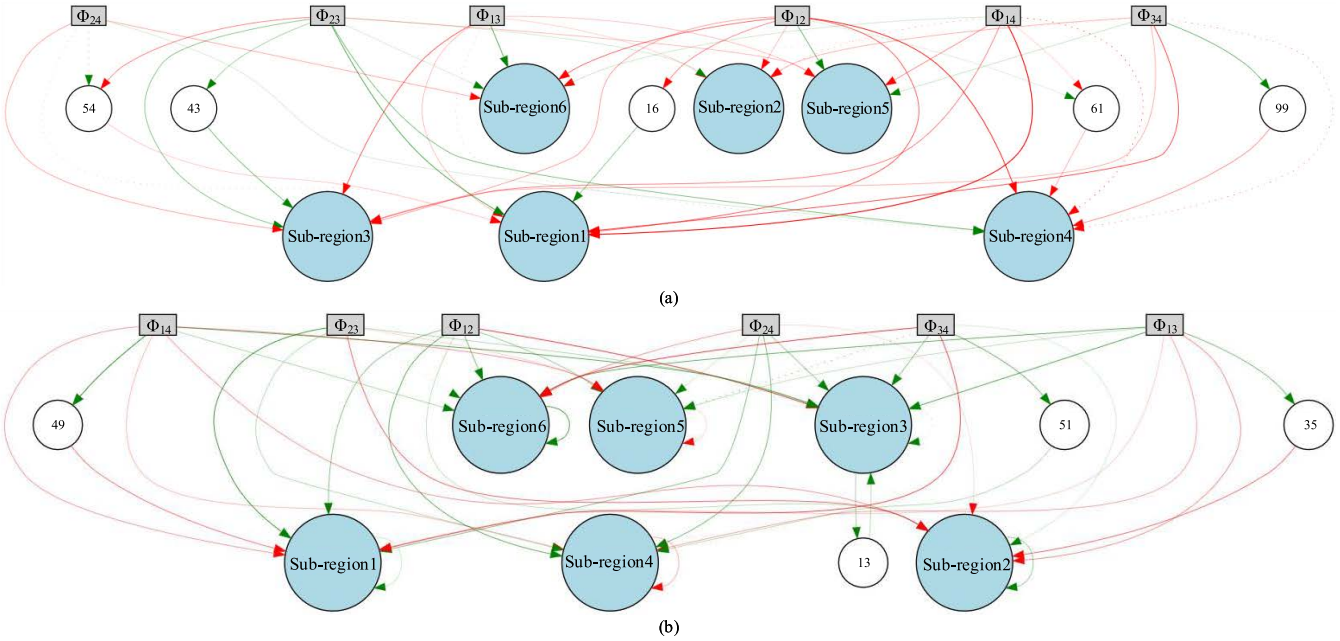

FIGURE 11. The NEAT networks (a) without recurrent link and (b) with recurrent link.

shown in Fig. 10. The element spacing is $\lambda/2$, and the number of snapshots is 200. The array element number M is 2×2 in this sub-section, so the input of the RNEAT algorithm is $[\Phi_{12}, \Phi_{13}, \Phi_{14}, \Phi_{23}, \Phi_{24}, \Phi_{34}]$ as according to Fig. 3. The NEAT networks without and with recurrent links are shown in Figs. 11(a) and 11(b), respectively. Fig. 11(a) has 40 links and 273 hidden neurons and Fig. 11(b) has 35 links, 5 recurrent links, and 148 hidden neurons. Compared with Fig. 11(a), Fig. 11(b) with recurrent links simplifies the structure of the neural evolution network, and the number of links and hidden nodes is less than Fig. 11(a). Furthermore, Figs. 12(a) and 12(b) exhibit the process changes of the NEAT networks without and with recurrent links. The NEAT with recurrent links requires 165 generations to successfully distinguish the 6 species, which demonstrates a faster process compared with the NEAT without recurrent links (requiring 240 generations).

Besides, a fitness function is set up for this network [38]. In order to minimize the general error between the network system's output and the actual output, the fitness function is given as

$$Fitness = \frac{1}{Error_{sum}} \tag{13}$$

where

$$Error_{sum} = \sqrt{\left(Out_1 - \hat{Out}_1\right)^2 + \left(Out_2 - \hat{Out}_2\right)^2 + \cdots}. \tag{14}$$

Variables Out and $\hat{Out}$ denote the output of the restricted scanning region neuroevolution network and the expected output, respectively. The expected outputs ($\hat{Out}_1$, $\hat{Out}_2$, …, $\hat{Out}_6$) are labeled as [(0,0,0,0,0,1), (0,0,0,0,1,0), …, (1,0,0,0,0,0)], which makes the calculation of Euclidean distance more reasonable. The fitness is an inverse of $Error_{sum}$. As it is shown in Fig. 13, the training process is finished till one of the network systems achieves a *Fitness* value of more than 1000 (an error of less than 0.001). The NEAT algorithm without recurrent links needs iterative updates 240 generations. In contrast, the NEAT algorithm with recurrent links only requires updating 165 generations. Besides, it can be observed from Figs. 13(a) and 13(b) that the NEAT algorithm with recurrent links exhibits a superior averaged *Fitness* value.

After the restricted scanning region neuroevolution network, the azimuth and elevation scan ranges of RNEAT-MUSIC are restricted as $[0°, 120°]$ and $[0°, 45°]$, respectively. For the hypothetical situation with two independent signals, RNEAT-MUSIC well estimates the number and direction of the incidence signal in sub-region, which can be used to estimate the independent signal source DOA effectively. A 3-D spectrum in azimuth and elevation is plotted in Fig. 14. The root mean square error (RMSE) of source is defined as

$$RMSE = \frac{1}{N_t}\sqrt{\sum_{i=1}^{N_t}\left[\left(\theta_i - \hat{\theta}_i\right)^2 + \left(\varphi_i - \hat{\varphi}_i\right)^2\right]}, \tag{15}$$

where N_t is the total examples number in the test set, and $\hat{\theta}_i$ and $\hat{\varphi}_i$ are the actual azimuth and elevation angles, respectively. θ_i and φ_i are the estimated azimuth and elevation angles, respectively. The RMSE simulation results with 10 Monte Carlo experiments are shown in Fig. 15, which exhibits the relationship between RMSE and the number

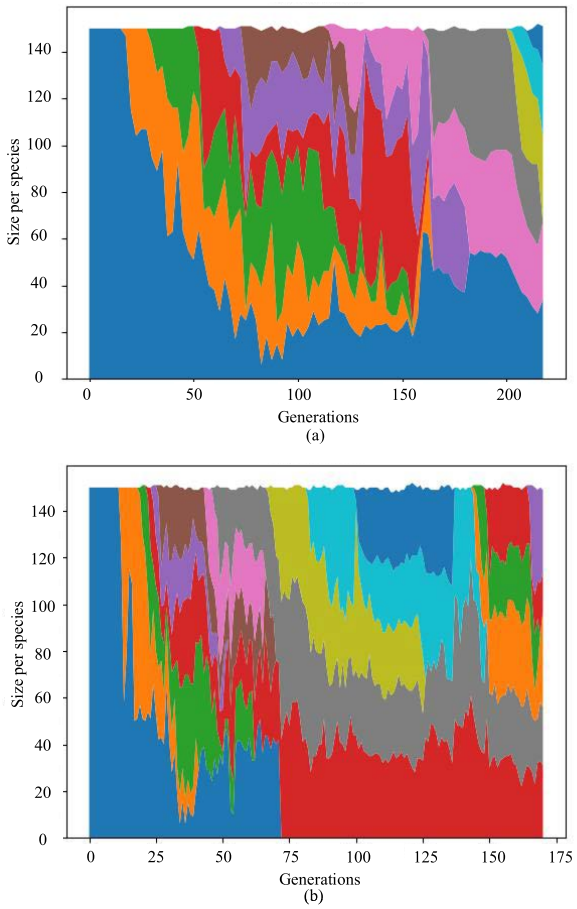

FIGURE 12. The process of species change (a) without recurrent links and (b) with recurrent links.

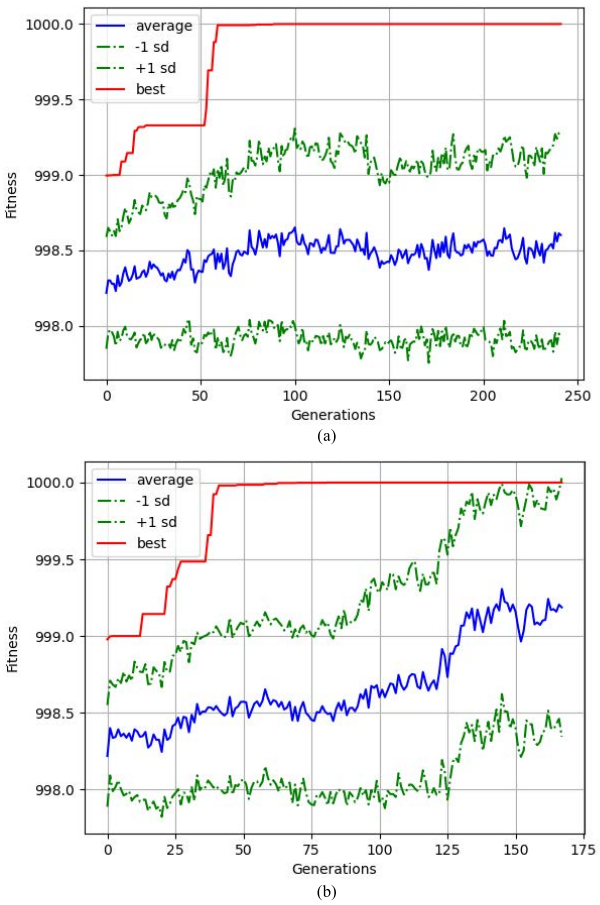

FIGURE 13. Fitness values in correspondence with iteration generations (a) without recurrent links and (b) with recurrent links. sd: standard deviation.

of receiver elements, the number of snapshots, and SNR, respectively.

B. THE RELATIONSHIP BETWEEN RNEAT-MUSIC AND THE NUMBER OF ARRAY ELEMENTS

This sub-section studies the relationship between RNEAT-MUSIC and the number of array elements. The array element numbers are selected as 5×5, 10×10, and 15×15. The simulated spatial spectrum for the relationship between RNEAT-MUSIC and the number of elements at 30° azimuth are shown in Fig. 16. As it can be seen from Fig. 16, the dashed, solid, and dash-dotted lines exhibit the case scenarios where the numbers of array elements equal to 5×5, 10×10, and 15×15, respectively. With the increase of array element number, the beam width of DOA estimation spectrum becomes narrower, and the directivity of the array becomes superior, i.e., the ability to distinguish spatial signals is enhanced. Hence, increasing the number of array element leads to more accurate estimations of DOA. Nevertheless, more array elements means more received data, heavier computation burden, as well as an excessive processing time. In Fig. 16, it can be seen that the directivity merit by increasing array elements becomes marginal when

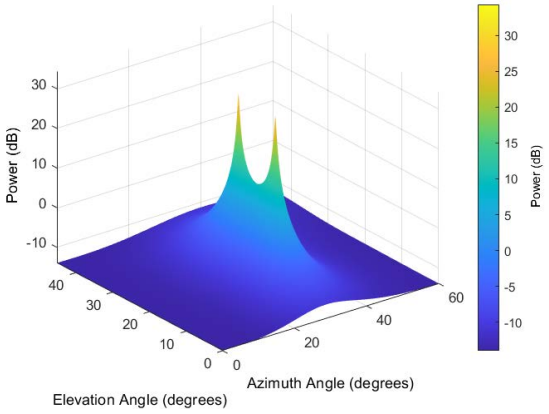

FIGURE 14. RNEAT-MUSIC spatial spectrum.

$M > 10 \times 10$, and the beam widths under $M = 10 \times 10$ and $M = 15 \times 15$ are comparable. Therefore, in practice, the number of elements should be properly selected considering both the accuracy of spectrum and the computational efficiency.

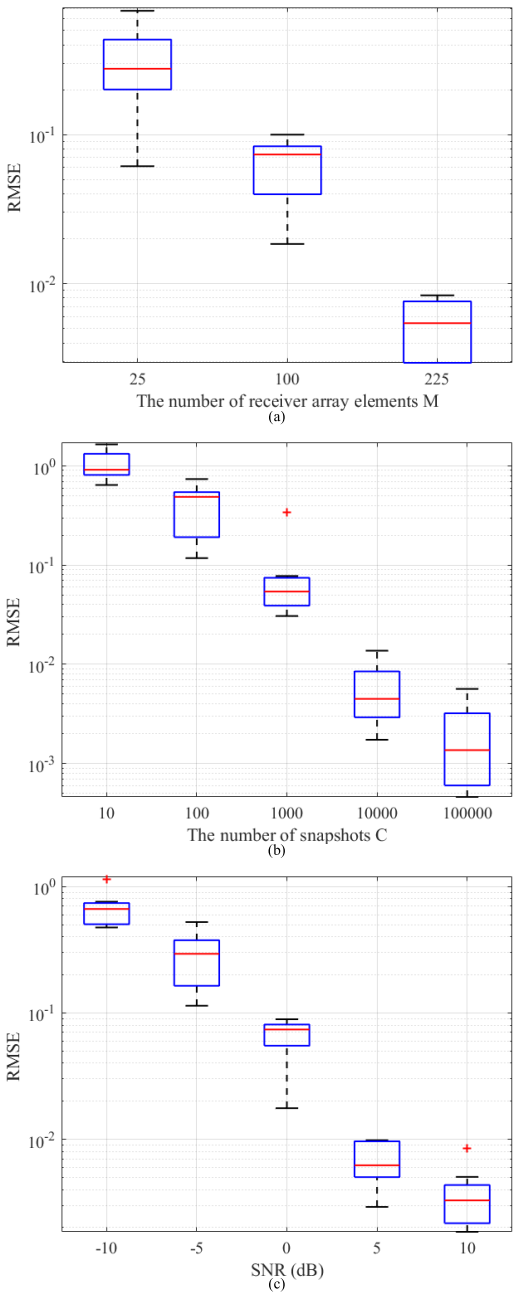

FIGURE 15. RMSE in correspondence with (a) the number of receiver array elements M, (b) the number of snapshots C, and (c) SNR.

C. THE RELATIONSHIP BETWEEN RNEAT-MUSIC AND THE ARRAY ELEMENT SPACING

In this sub-section, the array spacing is set to $\lambda/4$, $\lambda/2$, and λ, with the other conditions remaining the same. Simulation spatial spectrum for the relationship between RNEAT-MUSIC and the array element spacing at 30° azimuth are shown in Fig. 17. As it can be seen from Fig. 17, the dashed, solid, and dash-dotted lines exhibit the case scenarios where the array element spacing equals to $\lambda/4$, $\lambda/2$, and λ, respectively. With the increase of array element spacing, the beam width of DOA estimation spectrum becomes narrower, and

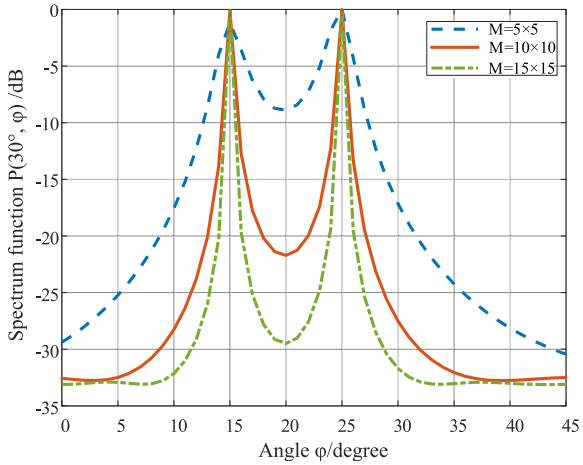

FIGURE 16. Simulated spatial spectrum for the relationship between RNEAT-MUSIC and the number of elements at 30° azimuth.

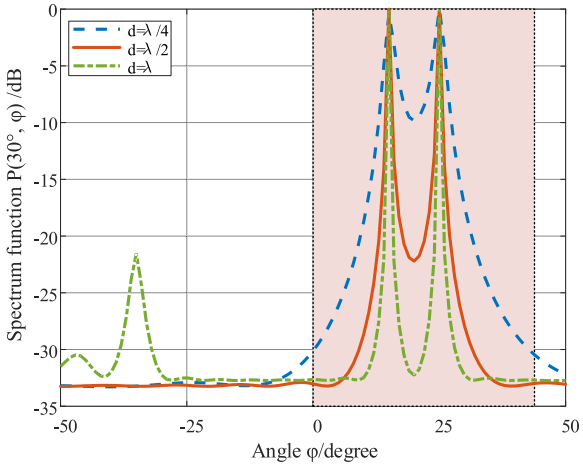

FIGURE 17. Simulated spatial spectrum for the relationship between RNEAT-MUSIC and array element spacing at 30° azimuth.

the directivity of the array becomes more accurate, i.e., the resolution of RNEAT-MUSIC improves with the increase of the array element spacing. On the other hand, the estimated spectrum may exhibit false peaks under the scenario that array element spacing is larger than half of the wavelength, as it can be observed from Fig. 17. Nevertheless, the proposed RNEAT-MUSIC can help to avoid false peaks, since the elevation scan region will be restricted in the range $[0°, 45°]$ with the restricted scanning region neuroevolution network.

D. THE RELATIONSHIP BETWEEN RNEAT-MUSIC AND THE NUMBER OF SNAPSHOTS

In this sub-region, various numbers of snapshots are selected as 10, 100, and 1000, with the other conditions remaining the same. The simulated spatial spectrum for the relationship between RNEAT-MUSIC and the number of snapshots at 30° azimuth are shown in Fig. 18. As it can be seen from Fig. 18, the dashed, solid, and dash-dotted lines exhibit the case scenarios where the number of snapshots equals to 10, 100,

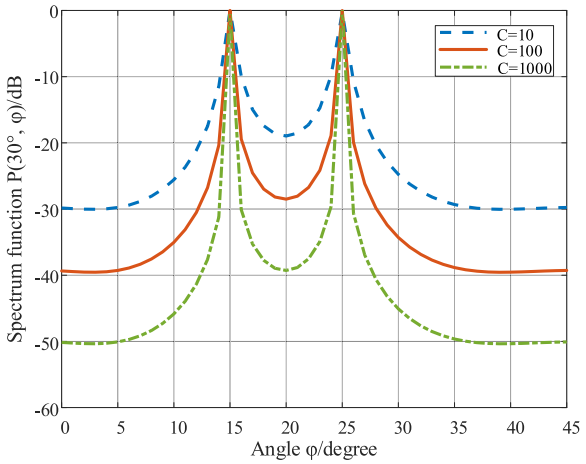

FIGURE 18. Simulated spatial spectrum for the relationship between RNEAT-MUSIC and the number of snapshots at 30° azimuth.

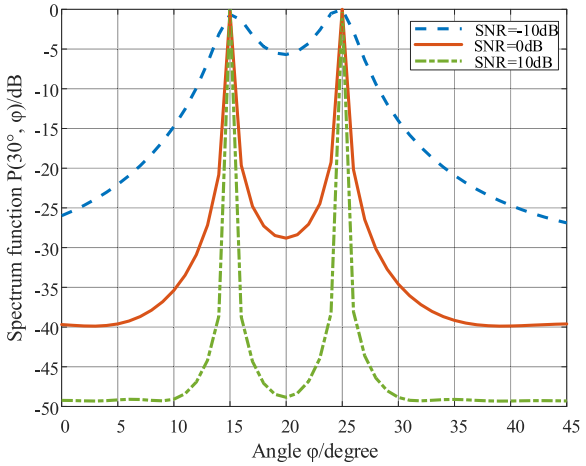

FIGURE 19. Simulated spatial spectrum for the relationship between RNEAT-MUSIC and SNR at 30° azimuth.

and 1000, respectively. With the increase of snapshot number, the beam width of DOA estimation spectrum becomes narrower, and the directivity of the array becomes more precise in resolution. The accuracy of the RNEAT-MUSIC algorithm is also increased with more snapshot number. Theoretically, the number of sample snapshots can be expanded to multiply the accuracy of DOA estimation. Nevertheless, more snapshots also means excessive processing data, heavy computational burden, and lengthy calculation period. Therefore, in practice, a reasonable snapshot number should be configured for RNEAT-MUSIC taking into account both the DOA estimation accuracy and the computational efficiency.

E. THE RELATIONSHIP BETWEEN RNEAT-MUSIC AND SNR

In this sub-section −10 dB, 0 dB, and 10 dB SNR are set. The relationship between RNEAT-MUSIC and SNR at 30° azimuth are shown in Fig. 19. In Fig. 19, the dashed, solid, and dash-doted lines exhibit the case scenarios where the SNR equals to −10 dB, 0 dB, and 10 dB, respectively.

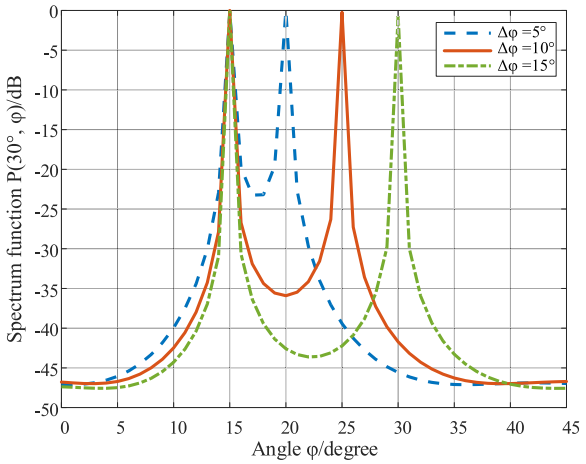

FIGURE 20. Simulated spatial spectrum for the relationship between RNEAT-MUSIC and incident angle difference at 30° azimuth.

With the increase of SNR value, the beam width of DOA estimation spectrum becomes narrower, and the accuracy of the RNEAT-MUSIC algorithm is enhanced. The value of SNR can affect the performance of high resolution DOA estimation algorithm directly. Under low SNR, the performance level of the RNEAT-MUSIC algorithm will decline. Thus, improving the estimation performance under low SNR is a main research topic for high resolution DOA estimation.

F. THE RELATIONSHIP BETWEEN RNEAT-MUSIC AND THE SIGNAL INCIDENT ANGLE DIFFERENCE

This simulation shows the relationship between RNEAT-MUSIC and the signal source incident angle difference, where the incident angle difference is 5°, 10°, and 15°, respectively. The spatial spectrum for the relationship between RNEAT-MUSIC and the signal incident angle difference at 30° azimuth are shown in Fig. 20. As it can be seen from Fig. 20, the dashed, solid, and dash-dotted lines exhibit the case scenarios where the incident angle differences equal to 5°, 10°, and 15°, respectively. With the increase of incident angle difference, the direction of the signal source becomes more clear and the resolution of RNEAT-MUSIC algorithm is improved.

V. CONCLUSION

This paper proposes a RNEAT-MUSIC algorithm to reduce the computational complexity of 2D-DOA. The improved NEAT algorithm combined with recurrent structure is used to minimize the neural network and set the weights automatically. The proposed method effectively estimates 2D-DOA by performance analysis, which is faster and can reduce more than 3/4 computational complexities compared with the traditional 2D-MUSIC algorithm. Simulation results verify the capability and reliability of the proposed method. The application prospect of RNEAT-MUSIC is successfully demonstrated in the area of 2D-DOA estimation.

REFERENCES

[1] A. Antón, I. García-Rojo, A. Girón, E. Morales, and R. Martínez, "Phase response calibration of a distributed antenna array for satellite acquisition," *IEEE Antennas Wireless Propag. Lett.*, vol. 15, pp. 1731–1734, 2016.

[2] A. Antón, I. García-Rojo, A. Girón, E. Morales, and R. Martínez, "Analysis of a distributed array system for satellite acquisition," *IEEE Trans. Aerosp. Electron. Syst.*, vol. 53, no. 3, pp. 1158–1168, Jun. 2017.

[3] S. K. Sharma, S. Chatzinotas, and B. Ottersten, "Satellite cognitive communications: Interference modeling and techniques selection," in *Proc. 6th Adv. Satell. Multimedia Syst. Conf. (ASMS), 12th Signal Process. Space Commun. Workshop (SPSC)*, Vigo, Spain, Sep. 2012, pp. 111–118.

[4] H. Shuai, S. Zhu, and C. Li, "Modeling and error accuracy analysis of three satellite interference source location system by low and high orbit," in *Proc. IEEE 9th Int. Conf. Electron. Inf. Emergency Commun. (ICEIEC)*, Beijing, China, Jul. 2019, pp. 1–7.

[5] S. Haykin, J. P. Reilly, V. Kezys, and E. Vertatschitsch, "Some aspects of array signal processing," *IEE Proc. F, Radar Signal Process.*, vol. 139, no. 1, pp. 1–26, Feb. 1992.

[6] M. Liu, J. Zhang, J. Tang, F. Jiang, P. Liu, F. Gong, and N. Zhao, "2-D DOA robust estimation of echo signals based on multiple satellites passive radar in the presence of alpha stable distribution noise," *IEEE Access*, vol. 7, pp. 16032–16042, 2019.

[7] J. W. Odendaal, E. Barnard, and C. W. I. Pistorius, "Two-dimensional superresolution radar imaging using the MUSIC algorithm," *IEEE Trans. Antennas Propag.*, vol. 42, no. 10, pp. 1386–1391, Oct. 1994.

[8] J. Li and R. T. Compton, "Two-dimensional angle and polarization estimation using the ESPRIT algorithm," *IEEE Trans. Antennas Propag.*, vol. 40, no. 5, pp. 550–555, May 1992.

[9] S. Ren, X. Ma, S. Yan, and C. Hao, "2-D unitary ESPRIT-like direction-of-arrival (DOA) estimation for coherent signals with a uniform rectangular array," *Sensors*, vol. 13, no. 4, pp. 4272–4288, Apr. 2013.

[10] F. Yan, M. Jin, and X. Qiao, "Low-complexity DOA estimation based on compressed MUSIC and its performance analysis," *IEEE Trans. Signal Process.*, vol. 61, no. 8, pp. 1915–1930, Apr. 2013.

[11] F. Yan, Z. Chen, M. Sun, Y. Shen, and M. Jin, "Two-dimensional direction-of-arrivals estimation based on one-dimensional search using rank deficiency principle," *Int. J. Antennas Propag.*, vol. 2015, no. 5, pp. 127621.1–127621.8, Dec. 2015.

[12] W. Nie, K. Xu, D. Feng, C. Wu, A. Hou, and X. Yin, "A fast algorithm for 2D DOA estimation using an omnidirectional sensor array," *Sensors*, vol. 17, no. 3, p. 515, Mar. 2017.

[13] W. Si, Y. Wang, C. Hou, and H. Wang, "Real-valued 2D MUSIC algorithm based on modified forward/backward averaging using an arbitrary centrosymmetric polarization sensitive array," *Sensors*, vol. 17, no. 10, p. 2241, Sep. 2017.

[14] L. Yaning, F. Juntao, R. Xinghao, and M. Le, "An improved MUSIC algorithm for DOA estimation of non-coherent signals with planar array," *J. Phys., Conf. Ser.*, vol. 1060, Jul. 2018, Art. no. 012026.

[15] H. Li, N. Zheng, X. Song, and Y. Tian, "Fast estimation method of space-time two-dimensional positioning parameters based on Hadamard product," *Int. J. Antennas Propag.*, vol. 2018, pp. 1–9, Mar. 2018.

[16] X. Dai, X. Zhang, and Y. Wang, "Extended DOA-matrix method for DOA estimation via two parallel linear arrays," *IEEE Commun. Lett.*, vol. 23, no. 11, pp. 1981–1984, Nov. 2019.

[17] X. Zeng, G. Chen, S. Jiao, S. Fu, and L. Dong, "High-accuracy and low-complexity DOA estimation algorithm for transmit-only diversity bistatic MIMO radar," *IEEE Access*, vol. 7, pp. 118278–118286, 2019.

[18] M. Feng, Z. Cui, Y. Yang, and Q. Shu, "A reduced-dimension MUSIC algorithm for monostatic FDA-MIMO radar," *IEEE Commun. Lett.*, vol. 25, no. 4, pp. 1279–1282, Apr. 2021.

[19] V. V. Reddy, M. Mubeen, and B. P. Ng, "Reduced-complexity super-resolution DOA estimation with unknown number of sources," *IEEE Signal Process. Lett.*, vol. 22, no. 6, pp. 772–776, Jun. 2015.

[20] X. Wang, W. Wang, and D. Xu, "Low-complexity ESPRIT–root-MUSIC algorithm for non-circular source in bistatic MIMO radar," *Circuits, Syst., Signal Process.*, vol. 34, no. 4, pp. 1265–1278, Apr. 2015.

[21] W. Liu, "Super resolution DOA estimation based on deep neural network," *Sci. Rep.*, vol. 10, no. 1, pp. 2045–2322, Nov. 2020.

[22] Z.-M. Liu, C. Zhang, and P. S. Yu, "Direction-of-arrival estimation based on deep neural networks with robustness to array imperfections," *IEEE Trans. Antennas Propag.*, vol. 66, no. 12, pp. 7315–7327, Dec. 2018.

[23] W. Hu, R. Liu, X. Lin, Y. Li, X. Zhou, and X. He, "A deep learning method to estimate independent source number," in *Proc. 4th Int. Conf. Syst. Informat. (ICSAI)*, Hangzhou, China, Nov. 2017, pp. 1055–1059.

[24] W. Zhu, M. Zhang, P. Li, and C. Wu, "Two-dimensional DOA estimation via deep ensemble learning," *IEEE Access*, vol. 8, pp. 124544–124552, 2020.

[25] B. Hu, M. Liu, F. Yi, H. Song, F. Jiang, F. Gong, and N. Zhao, "DOA robust estimation of echo signals based on deep learning networks with multiple type illuminators of opportunity," *IEEE Access*, vol. 8, pp. 14809–14819, 2020.

[26] M. Chen, Y. Gong, and X. Mao, "Deep neural network for estimation of direction of arrival with antenna array," *IEEE Access*, vol. 8, pp. 140688–140698, 2020.

[27] M. Agatonovic, Z. Stankovic, I. Milovanovic, N. Doncov, L. Sit, T. Zwick, and B. Milovanovic, "Efficient neural network approach for 2D DOA estimation based on antenna array measurements," *Prog. Electromagn. Res.*, vol. 137, pp. 741–758, 2013.

[28] S. Ruder, "An overview of gradient descent optimization algorithms," Sep. 2016, *arXiv:1609.04747*.

[29] H. Huang, J. Yang, H. Huang, Y. Song, and G. Gui, "Deep learning for super-resolution channel estimation and DOA estimation based massive MIMO system," *IEEE Trans. Veh. Technol.*, vol. 67, no. 9, pp. 8549–8560, Sep. 2018.

[30] R. Takeda and K. Komatani, "Discriminative multiple sound source localization based on deep neural networks using independent location model," in *Proc. IEEE Spoken Lang. Technol. Workshop (SLT)*, San Diego, CA, USA, Dec. 2016, pp. 603–609.

[31] S. Adavanne, A. Politis, and T. Virtanen, "Direction of arrival estimation for multiple sound sources using convolutional recurrent neural network," in *Proc. 26th Eur. Signal Process. Conf. (EUSIPCO)*, Rome, Italy, Sep. 2018, pp. 1462–1466.

[32] E. Galvan and P. Mooney, "Neuroevolution in deep neural networks: Current trends and future challenges," *IEEE Trans. Artif. Intell.*, vol. 2, no. 6, pp. 476–493, Dec. 2021.

[33] K. O. Stanley and R. Miikkulainen, "Evolving neural networks through augmenting topologies," *Evol. Comput.*, vol. 10, no. 2, pp. 99–127, Jun. 2002.

[34] P. Pal and P. P. Vaidyanathan, "Nested arrays: A novel approach to array processing with enhanced degrees of freedom," *IEEE Trans. Signal Process.*, vol. 58, no. 8, pp. 4167–4181, Aug. 2010.

[35] F. G. Yan, M. Jin, S. Liu, and X. L. Qiao, "Real-valued MUSIC for efficient direction estimation with arbitrary array geometries," *IEEE Trans. Signal Process.*, vol. 62, no. 6, pp. 1548–1560, Mar. 2014.

[36] W. Zhu and M. Zhang, "A deep learning architecture for broadband DOA estimation," in *Proc. IEEE 19th Int. Conf. Commun. Technol. (ICCT)*, Xi'an, China, Oct. 2019, pp. 244–247.

[37] G. Papageorgiou, M. Sellathurai, and Y. Eldar, "Deep networks for direction-of-arrival estimation in low SNR," *IEEE Trans. Signal Process.*, vol. 69, pp. 3714–3729, 2021.

[38] D. Loiacono, "Gene I. Sher: Handbook of neuroevolution through Erlang," *Genet. Program. Evolvable Mach.*, vol. 15, no. 1, pp. 109–110, 2014.

[39] G. Xu and T. Kailath, "Fast subspace decomposition," *IEEE Trans. Signal Process.*, vol. 42, no. 3, pp. 539–551, Mar. 1994.

[40] K. O. Stanley and R. Miikkulainen, "Efficient evolution of neural network topologies," in *Proc. Congr. Evol. Comput. (CEC)*, vol. 2, Honolulu, HI, USA, 2002, pp. 1757–1762.

[41] R. Miikkulainen, J. Liang, E. Meyerson, A. Rawal, D. Fink, O. Francon, B. Raju, H. Shahrzad, A. Navruzyan, N. Duffy, and B. Hodjat, "Evolving deep neural networks," 2017, *arXiv:1703.00548*.

[42] *NEAT Overview*. Accessed: Nov. 20, 2021. [Online]. Available: https://neat-python.readthedocs.io/en/latest/neat_overview.html

[43] P. J. Angeline, G. M. Saunders, and J. B. Pollack, "An evolutionary algorithm that constructs recurrent neural networks," *IEEE Trans. Neural Netw.*, vol. 5, no. 1, pp. 54–65, Jan. 1994.

YUNFENG LI (Student Member, IEEE) was born in Linyi, China, in 1995. She received the B.Sc. degree in electronic information science and technology from Shandong Normal University, Shandong, China, in 2017. She is currently pursuing the Ph.D. degree with the Key Laboratory of Electronics and Information Technology for Space Systems, National Space Science Center (NSSC), University of the Chinese Academy of Sciences (UCAS). She was a Visiting Ph.D. student in RF and mm-wave circuits and systems with the Department of Electronic Systems, Aalborg University, Denmark, from March 2019 to March 2020, where she was also a Research Assistant in RF and mm-wave circuits and systems with the Department of Electronic Systems, from March 2020 to March 2021. Her research interests include digital pre-distortion techniques, millimeter wave antenna design, and DOA signal processing. She serves as a Reviewer for IEEE Access.

YONGHUI HUANG was born in Anshan, China. He received the B.Sc. degree in electronics engineering from the Tsinghua University of Beijing, China, in 1998, the M.Sc. degree in aero-spacecraft design from the University Chinese Academy of Sciences of Beijing, China, in 2001, and the Ph.D. degree in wireless communication from Aalborg University, Aalborg, Denmark, in 2008.

He was an Engineer at Datang Mobile of Beijing, China, from 2001 to 2002. From 2002 to 2011, he worked as a Postdoctoral Researcher and a Research Assistant with Aalborg University. He is currently a Professor with the National Space Science Center, Chinese Academy of Science, Beijing, China. His current research interests include deep space communication, satellite wireless communication, phased array antenna, and transmitter linearization. He is a TPC Member of IEEE CCET and IEEE WiSEE.

GERT FRØLUND PEDERSEN (Senior Member, IEEE) was born in 1965. He received the B.Sc. and E.E. (Hons.) degrees in electrical engineering from the College of Technology in Dublin, Dublin Institute of Technology, Dublin, Ireland, in 1991, and the M.Sc. (E.E.) and Ph.D. degrees from Aalborg University, Aalborg, Denmark, in 1993 and 2003, respectively.

He has also worked as a Consultant for developments of more than 100 antennas for mobile terminals, including the first internal antenna for mobile phones, in 1994, with lowest SAR, first internal triple-band antenna, in 1998, with low SAR and high TRP and TIS, and lately various multiantenna systems rated as the most efficient on the market. He has worked most of the time with joint university and industry projects and have received more than 21 M$ in direct research funding. Since 1993, he has been with Aalborg University, where he is currently a Full Professor, heading the Antennas, Propagation and Millimeter-Wave Systems Laboratory with 25 researchers. He is also the Head of the Doctoral School on Wireless Communication with some 40 Ph.D. students enrolled. He is currently the Project Leader of the RANGE Project with a total budget of over eight M$ investigating high performance centimetre/millimeter-wave antennas for 5G mobile phones. He has been one of the pioneers in establishing over-the-air measurement systems. The measurement technique is now well established for mobile terminals with single antennas and he was chairing the various COST groups with liaison to 3GPP and CTIA for over-the-air test of MIMO terminals. He is currently involved in MIMO OTA measurement. He has published more than 500 peer reviewed papers, six books, 12 book chapters, and holds over 50 patents. His research interests include radio communication for mobile terminals, especially small antennas, diversity systems, propagation, and biological effects.

MING SHEN (Senior Member, IEEE) was born in Yuxi, China. He received the M.Sc. degree in electrical engineering from the University of Chinese Academy of Sciences (UCAS), Beijing, China, in 2005, and the Ph.D. degree in wireless communications from Aalborg University, Aalborg, Denmark, in 2010, with the Spar Nord Annual Best Thesis nomination.

He is currently an Associate Professor in RF and mm-wave circuits and systems with the Department of Electronic Systems, Aalborg University. He has 20 years experience in RF and millimeter wave circuits and systems, including 12 years experience in CMOS RF/mixed-signal IC design. His current research interests include circuits and antennas for 5G and satellite communications, low power CMOS RF and millimeter wave circuits and systems, circuits and systems for biomedical imaging, and artificial intelligence. He is the grant holder and a PI of three Danish national research projects, and the management committee member substitute from Denmark in the EU COST Action IC1301 with the aim to gather the international efforts and address efficient wireless power transmission technologies. He is a member of the TPC Member of IEEE NORCAS and serves as a Reviewer for IEEE and Kluwer.